Saudi Pharmaceutical Journal 27 (2019) 112–125

Contents lists available at ScienceDirect

Saudi Pharmaceutical Journal

journal homepage: www.sciencedirect.com

Original article

Transdermal patches loaded with L-cysteine HCL as a strategy for protection from mobile phone emitting electromagnetic radiation hazards

Samia M. Omar [a,b,*], Mohamed Nasr [a], Diana A. Rafla [c]

[a] Department of Pharmaceutics, Faculty of Pharmacy, Helwan University, Cairo, Egypt
[b] Department of Pharmaceutics, Faculty of Pharmacy, Ahram Canadian University, Giza, Egypt
[c] Pharmacist at Helwan General Hospital, Cairo, Egypt

ARTICLE INFO

Article history:
Received 11 February 2018
Accepted 1 September 2018
Available online 5 September 2018

Keywords:
Electromagnetic radiation
Mobile phone hazards
L-cysteine
Transdermal patches
Silicone transdermal patches
Glutathione

ABSTRACT

Mobile phone usage has been increased in the last few years emitting electromagnetic radiation (EMR), which disturbs normal cellular processes via oxidative stress. L-cysteine, a glutathione precursor, prevents oxidative damage. Transdermal patches (TDPs) loaded with L-cysteine hydrochloride (L-CyS-HCL) were fabricated by dispersion of L-CyS-HCL 5% w/w and different concentrations of sorbitol as a plasticizer in room-temperature vulcanizable synthetic silicone matrices (RTV-Si). The effect of sorbitol on patch physicochemical parameters was assessed; *in-vitro* L-CyS-HCL release profiles and *ex-vivo* permeation were studied. Pharmacokinetic parameters of endogenous synthetized *in-vivo* glutathione, after receiving IV bolus dose of L-CyS-HCl and L-CyS-HCl-RTV-Si-TDPs were studied in rat model. The influence of L-CyS-HCL-RTV-Si-TDPs against damaging effects of mobile phone EMR on rats' blood and brain tissues was studied. The results revealed that patch plasticity, intensity reflections, surface porosity, L-CyS-HCL release rate and skin permeation increased with increasing sorbitol concentration. Pharmacokinetic profile for IV dose and L-CyS-HCl-RTV-Si-TDPs revealed that the L-CyS-HCl-RTV-Si-TDPs provided a sustained glutathione plasma concentration–time profile over entire patch application. High significant differences in biological parameters (blood and brain samples) were observed for radiated rats using the patch in study compared with positive control rats. Promising long-term strategy for protection against mobile phone hazards was obtained.

1. Introduction

Nowadays technology is the lifeline of modern day society. The day life usage of electronic equipment makes us more liable to electromagnetic radiation (EMR). The growth of mobile phone telecommunications has increased the scientific awareness on biological effects of EMR emitted from cellular phones and their consequences on human health. Ozguner et al. (2005) have reported that EMR of cellular phones may affect biological systems by increasing free radicals that enhancing lipid peroxidation and by changing the antioxidant defense systems of tissues, thus leading to oxidative stress (Ozguner et al., 2005). Reactive oxygen species (ROS) are known as unpaired electron of molecular oxygen react to form highly reactive species, generated from enzymatic and non-enzymatic sources that lead to oxidative stress. Many pathological conditions including cancer, neurological disorders, atherosclerosis and hypertension are contributed to oxidative stress. In addition, as microwaves in the frequency range of 800–1000 MHz can commonly penetrate the cranium, near 40% of the absorbed microwaves can extent through the deep brain (Klemm and Troester, 2006).

Several trials have been made to study the protective effect of different natural antioxidants as vitamins and melatonin hormone against mobile phone biological hazards (Guney et al., 2007; Kerman and Senol, 2012). Recently, many studies have established the protective effect of N-acetyl cysteine/L-CyS as powerful antioxidant for ameliorating the effects of mobile phone radiation

* Corresponding author at: Department of Pharmaceutics, Faculty of Pharmacy, Ahram Canadian University, Giza, Egypt.
E-mail address: omarsamia3@hotmail.com (S.M. Omar).
Peer review under responsibility of King Saud University.

Production and hosting by Elsevier

https://doi.org/10.1016/j.jsps.2018.09.004
1319-0164/

(Abdel-Rahman, 2004; Ozgur et al., 2010). However, the principal defense system against ROS was previously studied, underlining that L-cysteine (L-CyS) plays a key-role in preventing oxidative damage, this action is partly due to direct antioxidant properties via its thiol function that can scavenge free radicals and certainly more significantly as a limiting precursor of reduced GSH (Li et al., 2002).

It has been recognized previously that, L-CyS crosses the erythrocyte membranes (influx and efflux processes) more efficiently than N-acetyl cysteine; hence it could be more effectively than N-acetyl cysteine in restoring the depleted intracellular free-SH level. Thus, under oxidative conditions L-CyS may be more efficient with faster response in protection against oxidative stress and in regeneration of GSH levels (Yildiz et al., 2009).

Transdermal patches (TDPs) as medicated adhesive patches, placed on the skin and deliver a specific drug dose through the skin reaching the bloodstream, are attractive method to avoid first-pass metabolism, lower fluctuations in plasma drug levels, targeting of the active ingredient for a local effect and good patient compliance. Room-temperature vulcanizable silicone (RTV-Si) has been used previously for TDPs preparations. Because elastomers are commercial polymers that offer unique biocompatibility characteristics and are not biodegradable, they are widely used in biomaterials, particularly in medical devices for drug delivery or controlled drug release; among medical grade silicones, polydimethylsiloxane not only satisfies the above standards but can also be used in skin topical applications and long term implants (Tsai and Chang, 2013).

The aim of the present work was to address the influence of L-cysteine hydrochloride loaded in room-temperature vulcanizable silicone transdermal patches (L-CyS-HCL-RTV-Si-TDPs) as a promising approach for protection against oxidative stress hazards produced by the use of mobile phone emitting electromagnetic radiation.

2. Materials and methods

2.1. Materials

Polydimethylsiloxane was purchased from Dow Corning Inc., (Midland, MI, USA), L-cysteine hydrochloride monohydrate, sorbitol and Ellman's reagent (DTNB) were purchased from Sigma Aldrich (St. Louis, USA), other chemicals were of analytical grade.

2.2. Preparation of RTV-Si-TDPs loaded with L-CyS-HCl

The method of RTV-Si-TDPs preparation was in agreement with that described recently (Tsai and Chang, 2013). Briefly, polydimethylsiloxane (a soft elastomer RTV-Si) was prepared by mixing the monomer, liquid (A) and the crosslinking promoting agent (platinum salt), liquid (B) at a ratio of 10:1 for A: B, w/w (F1). For preparation of L-CyS-HCl-loaded RTV-Si-TDPs, 5% L-CyS-HCl and different concentrations of sorbitol (0%, 5%, 10%, 15% and 20%w/w of patch weight) were levigated with liquid B and then mixed with liquid A to prepare F2, F3, F4, F5 and F6 respectively. The mixtures were immediately poured over a Teflon mold and kept overnight for dryness at room temperature.

2.3. Evaluation of the prepared RTV-Si -TDPs

2.3.1. Thickness

The thickness of TDPs were determined using (Zwick Roell Tensile Testing Proline, Germany), at different points of the patch.

2.3.2. Tensile strength and % elongation

Tensile strength, the maximum stress applied to a point where the patch breaks, as well as % elongation, a measure of the capacity of a patch to deform prior to failure, were determined for tested elastomer specimens according to the manner described previously, using tensile strength testing apparatus (Zwick Roell Tensile Testing Proline, Germany), (Bharkatiya et al., 2010). Yield points (Y) were recorded as an indication of tensile strength. Sample's tensile strength was calculated by dividing the load at break (Newton) by the cross sectional area of the specimen (m2) and expressed in MPa. In addition, the changes in the length of the strips occurring by means of increasing stress were recorded as % elongation (Raghavendra et al., 2000). At least five replicates were done for each formulated patch.

2.3.3. X-ray diffraction

To inspect the effect of sorbitol embedded in TDPs on crystalline nature of silicon patches. X-ray diffraction patterns were detected for (F1, F2, F3 and F5) using X-ray diffractometer (Model: XPERT–PRO–PANalytical–Netherland). The diffractograms were recorded at room temperature under the following conditions: 45 kV voltage, 30 mA current, at 0.02° steps, counting rate of 0.5 s/step with Cu tube anode and scattering angle of (2θ) ranged (4–80°) and λ 1.54 Å.

Bragg's law could be used to calculate the distance between atomic layers in the polymeric crystal of different patches (d-spacing) using the following equation (Shaikh et al., 2007):

$$n\lambda = 2d\sin\theta \quad (1)$$

where n is an integer, λ is the wavelength of the incident X-ray beam, d is the distance between atomic layers in the polymeric crystal of different patches (d-spacing) and Theta Θ is angle of incidence of X-ray beams.

2.3.4. Evaluation of surface porosity

The effect of sorbitol on the surface porous texture of different prepared RTV-Si-TDPs was examined using field emission high vacuum mode scanning electron microscope (FE-SEM, Quanta FEG 250, Holland) (Wang et al., 2016).

2.4. In-vitro release study

The *in-vitro* L-CyS-HCl release from prepared RTV-Si-TDPs was performed by using Franz diffusion cell (with a donor compartment diameter of 2.25 cm) as described previously (Patel et al., 2012). Four cm^2 L-CyS-HCl-loaded RTV-Si-TDPs samples equivalent to 20 mg of L-CyS-HCl were tested for drug release. A volume of 10 ml of simulated sweat medium (SSW3) pH 5.4 (Marques et al., 2011) at 37 ± 1 °C was placed in the receptor compartment as a release medium (water solubility of L-CyS-HCl is 50 mg/ml). At predetermined time intervals, 250 μl samples were withdrawn from the release medium for L-CyS-HCl analysis and replaced with fresh medium at the same temperature for a period of 24 h.

2.4.1. Determination of released L-CyS-HCl from RTV-Si-TDPs using Ellman's reaction

The released L-CyS-HCl was determined using Ellman's reaction following the method described previously (Bernkop-Schnürch et al., 2003). The reaction was allowed to proceed for 2 h at room temperature. Samples were analyzed spectrophotometrically for released L-CyS-HCl using UV/visible spectroscopy (Jasco spectrophotometer, Japan). Results were expressed as cumulative release percent of three replicates.

Difference factor (f_1), as a pair-wise procedure, was calculated to study the dissimilarity between the release profiles of L-CyS-HCl

from F3, F4, F5 and F6 compared with that of F2 as a reference, using the following equation (Moore, 1996):

$$f_1 = \left[\frac{[\sum_{t=1}^{n}|R_t - T_t|]}{\sum_{t=1}^{n} R_t}\right] \times 100 \quad (2)$$

where the f_1 represents the percent difference between the two curves at each time point and is a measurement of the relative error between the two curves, n is the number of time points, R_t is the released value of the reference at time t, and T_t is the released value of the test at time t. Value for f_1 more than 15.0 shows dissimilarity of the two profiles.

2.4.2. Release kinetics and mechanism study

The *in-vitro* release data obtained was subjected to various mathematical models (zero order, first order and second order) to predict the kinetics of the drug release. The best-fitted model was selected according to the regression coefficient (r^2) value. For investigating the mechanism of release behavior of L-CyS-HCl from the prepared RTV-Si-TDPs, the data were analyzed using Higuchi diffusion equations and Korsmeyer-Peppas release model, given by the following equation (Korsmeyer et al., 1983):

$$M_t/M_\infty = kt^n \quad (3)$$

where M_t/M_∞ represents the fractional drug released at time t, K was the kinetic constant of drug/polymer system and n was the release exponent characterizing the release mechanism.

The model proposed by Peppas and Sahlin was also applied for studying the release mechanism of L-CyS-HCl from different formulations using the following equation (Peppas and Sahlin, 1989):

$$M_t/M_\infty = k_1 t^m + k_2 t^{2m} \quad (4)$$

where K_1 and K_2 were obtained from nonlinear regression curve fitting of the release data using GraphPad prism 4 (GraphPad Software, San Diego, CA, USA). In this model, the mechanism of drug release could be confirmed by means of the values of relaxation (R) and Fickian (F) ratio contributions (R/F), according to the heuristic model developed previously (Peppas and Sahlin, 1989)

$$R/F = K_2/K_1 t^m \quad (5)$$

2.5. Skin permeation study of L-CyS-HCl from RTV-Si-TDP through excised rat dorsal skin

2.5.1. Experimental animals

Male Wistar Albino rats weighing 140 ± 20 g were purchased from the animal house of the Egyptian Company for Production of Vaccines, Sera and Drugs (EGY VAC), (Helwan, Cairo, Egypt). National Institutes of Health (NIH) guidelines for the care and use of laboratory animals have been followed; besides, animal research protocol has been approved by the Animal Ethics Committee of Faculty of Pharmacy, Helwan University, and committee regulations were followed during the study. Rats were housed in cages away of near sources of EMR and maintained on stock diet and kept under fixed appropriate conditions of housing and handling till the experimental period, with free access to standard laboratory food and tap water, at a constant room temperature of 25 °C and a natural day/night cycle. The sacrificed animals were safely removed according to regulations for disposal of biological wastes.

2.5.2. Skin permeation study

Rat dorsal skin was freshly used for the study of L-CyS-HCl skin permeation from RTV-Si-TDP. One day prior to the experiment, hair was removed with a depilatory cream and rinsed well with water. On experiment day, rats were sacrificed and 5 cm × 5 cm pieces of skin were excised from the dorsal region and subcutaneous fat and connective tissue were carefully removed. Each skin specimen was inspected for damage using a magnifying lens, and hydrated in isotonic phosphate buffered saline (PBS, pH 7.4). Franz diffusion cells were used for the permeation experiments. Excess PBS was removed from the surface of the skin by gently dabbing with lint-free tissue paper. The study was performed on the selected L-CyS-HCl loaded RTV-Si-TDP (F2, F3 and F5). Four cm^2 of L-CyS-HCl-RTV-Si-TDP, equivalent to 20 mg L-CyS-HCl, was placed on the skin surface in the donor compartment. Receptor compartment was filled with 10 ml of PBS, pH 7.4. A temperature of 37 ± 1 °C was maintained with continuous stirring at 600 rpm using magnetic stirrer. At predetermined time intervals, 250 μL aliquots were removed from receptor compartment and the receptor phase was replenished to maintain a constant volume. Permeated L-CyS-HCl in the receptor phase was determined as mean of three replicates using Ellman's reaction as stated before.

2.5.3. Permeation data analysis

The cumulative amounts of L-CyS-HCl permeated through excised skins were plotted as a function of time. The slope and intercept of the linear portion of the plot were derived by regression. The permeation rate at steady-state (J, mg/cm^2/h) was calculated as the slope divided by the skin surface area. The intercept on the X-axis was taken as the lag time (T_L, h). The permeation rate was determined using the following equation:

$$J = \frac{1}{A}\left(\frac{dQ}{dt}\right)_{ss} = C_0 K_P \quad (6)$$

where J is the permeation rate at steady-state (mg/cm^2/h), A is the effective diffusion area (cm^2), (dQ/dt)ss is the amount of drug permeated through the skin per unit time at steady-state (mg/h), C_0 is the drug concentration in the patch (w/w) and K_p is the permeability coefficient (cm/h) (Barry, 1983)

2.6. In-vivo permeation and pharmacokinetics study of L-CyS-HCl-RTV-Si-TDP in rats

The study was performed on the selected L-CyS-HCl-RTV-Si-TDP (F5) using adult Wistar Albino rats model weighing 140 ± 20 g. Rats were randomly divided into three groups of 8 rats each: control group (untreated group), and L-CyS-HCL loaded RTV-Si-TDP (F5) receiving group, and 20 mg L-CyS-HCL in I.V. bolus dose receiving group. One day prior to the experiment, the hair of abdominal region was removed with a depilatory cream and rinsed well with water, 16 cm^2 patches (equivalent to 80 mg of L-CyS-HCl) were adhered to the hairless abdominal region, blood samples were withdrawn from rats each six hours for a period of seven days. Blood samples were analyzed for total GSH level (endogenously induced by the effect of L-CyS-HCl) by Ellman's reaction spectrophotometrically at λ_{405nm}. As well, non-compartment pharmacokinetic parameters (PKPs) of endogenous induced GSH in rats' plasma were estimated after baseline correction, using software Kinetica version 5.1 (Thermo Scientific, USA).

Relative bioavailability of the patch was evaluated against 20 mg I.V. bolus dose using the following equation (Borgström and Kågedal, 1990):

$$\text{Relative bioavailability of the patch (F)} = \frac{\text{AUCinf(patch)}}{\text{AUCinf(I.V.)}} \cdot \frac{\text{Dose(I.V.)}}{\text{Dose(patch)}} \quad (7)$$

2.7. In-vivo evaluation of protective effect of L-CyS-HCl-RTV-Si-TDPs against oxidative stress hazards of mobile phone emitting EMR

Experiments were performed on adult male Wistar Albino rats' model weighing 140 ± 20 g. Where, the effects of microwave emit-

ted from mobile phones on the *in-vivo* CNS neuronal cells, as well as blood and biological parameters were studied and the protagonist of L-CyS-HCL as a prophylactic treatment was ascertained.

2.7.1. Microwave generator system

The electromagnetic waves signals were generated by a microwave generator and the field densities in the chamber were measured by the microwave analyzer (ROHDE & SCHWARZ ZVA67 vector network analyser 10 MHz–67 GHz - USA), Fig. 1, supplied from the electronic research Centre, National Research Center (Dokki, Cairo, Egypt). The radiation frequency was set to be 900 MHz. mimicking mobile phone, and the electromagnetic waves were radiated through horn antenna to caged rats.

2.7.2. Experimental design

The experimental design followed that described recently (El-Bediwi et al., 2013). The rats were loaded into plastics cage with a distance of 30 cm away from the irradiation source. Rats were randomly divided into nine groups of 8 rats each: negative control group (unexposed to radiation and untreated with L-CyS-HCL) (Group 1), positive control group (exposed to radiation and untreated with L-CyS-HCL) (Group 2), and seven prophylactic treated groups (Group 3 to 9). Six of them (group 3, 4, 5, 7, 8 and 9) received one milliliter IV Injection of different concentrations of L-CyS-HCL (5, 10, 20, 30, 40 and 50 mg/ml) using L-CyS-HCl monohydrate (50 mg/ml) I.V Injection, (USP, Sandoz Inc.) diluted with 5% IV dextrose. In addition, L-CyS-HCL loaded RTV-Si-TDPs (F5) equivalent to 80 mg dose (Group 6). Rat dose was calculated from previously reported safely human doses of L-CyS-HCl derivatives (600–1800 mg/day) (Entzian, 1998).

After 2 h post treatment with 5 mg, 10 mg and 20 mg IV of L-CyS-HCL; as well as after 2 days post treatment with L-CyS-HCL-RTV-Si-TDPs (F5), Group 2, 3, 4, 5 and 6, respectively; positive control group as well as prophylactic treated groups were similarly exposed to 900 MHz RF/MW continuous fields for continuous four hours (short term exposure), with installed temperature and humidity through-out the duration of experiment.

2.7.3. Effect of electromagnetic radiation on red blood cells (Hematological studies)

2.7.3.1. Osmotic fragility test. In hematological studies, the osmotic fragility test provides an indication of the ratio of surface area/volume of the erythrocyte (expressed as percentage hemolysis) (Alhassan et al., 2010). In the osmotic fragility test, whole blood (exactly 0.02 ml of blood sample) was added to 10 ml of varying concentrations of sodium chloride solutions (0.1, 0.2, 0.3, 0.4, 0.5, 0.6, 0.7, 0.8 and 0.9%), at pH 7.4. The concentration of hemoglobin in the supernatant solution was measured spectrophotometrically at $\lambda_{540\ nm}$. The osmotic fragility expressed as percentage haemolysis was calculated using the following formula (Alhassan et al., 2010):

$$\text{Percent Haemolysis} = \frac{\text{Optical density of tested sample}}{\text{Optical density of blood in deionized water}} \times 100 \quad (8)$$

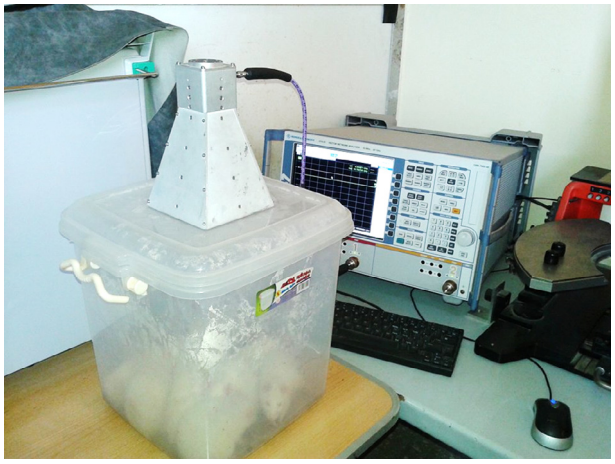

Fig. 1. Microwave generator with microwave analyzer (ROHDE & SCHWARZ ZVA67 vector network analyzer 10 MHz–67 GHz - USA). The electromagnetic waves signals generate a radiation frequency at 900 MHz. mimicking mobile phone, and the electromagnetic waves were radiated through horn antenna to caged rats.

2.7.3.2. Blood picture. At the end of irradiation period, blood samples were collected in sterile heparinized anticlotting tubes (VOMA MED, LH), and samples were used in evaluation of blood profile using automated blood analyzer MSLAB07 (China, mainland) (Alghamdi and ElGhazaly, 2012). Blood profile comprised in: (1) Complete blood count including percentage lymphocytes (% LY), platelets (PLT) count, red blood corpuscles count (RBCs), hemoglobin (Hb) and hematocrit (Hct). As well as, (2) Measurements of RBCs Indices comprising: mean cell volume (MCV), mean corpuscular hemoglobin (MCH) and mean corpuscular hemoglobin concentration (MCHC).

2.7.3.3. Blood biochemical analysis. The methods were in agreement with that described previously (Meral et al., 2007). Whole blood samples were collected into heparinized tubes for estimation of reduced GSH levels and blood serum malondialdehyde (MDA) levels.

- ***Determination of reduced GSH***

Protein was removed from collected blood samples using trichloroacetic acid (Akerboom and Sies, 1981). Aliquots of the supernatant liquid were analyzed for GSH content using freshly prepared Ellman's reagent, and the mixtures were measured spectrophotometrically following the method described previously (Błońska-Sikora et al., 2012; Rover et al., 2001).

- ***Malondialdehyde level determination***

Malondialdehyde (MDA) is a degradative product of peroxidation of polyunsaturated fatty acids in cell membrane, which is mostly used as an oxidative stress marker (Yurekli et al., 2006). MDA level was determined in blood samples according to the method described previously, using the spectrophotometric measurement of the formed MDA coloured complex with thiobarbituric acid at λ_{532nm} (Kerman and Senol, 2012).

2.8. Histological study of different brain tissue samples

2.8.1. Tissue sampling and preparation

For the histological study, rats from different groups were sacrificed under deep anesthesia and their brains were dissected out to obtain the chosen areas (cortex, hypothalamus and striatum). Paraffin-embedded rat brain sections were prepared according to routine procedures. Briefly, suitable pieces were collected and fixed in 10% formol saline for twenty-four hours. Washing was done under tap water then the pieces were dehydrated in ascending series of alcohols (methyl, ethyl and absolute ethyl), cleared in xylene and embedded in paraffin wax for tissue blocks preparation. Sections of 5 μm thickness were stained with hematoxylin & eosin.

2.8.2. Histopathological examination

Routine histopathological examination through light electric microscope (Jackson and Blythe, 2013) was performed. Any alterations compared to the normal structure were registered. Cells showed nuclear pyknosis, degeneration and vacuolization with cytoplasmic oedema and focal gliosis were regarded as positive. Labeling Index (LI) was calculated according to the following formula (Zhu et al., 2008):

$$LI = (\text{positive cell number}/\text{total cell count}) \times 100 \quad (9)$$

2.9. Statistical data analysis

Results were expressed as mean standard deviation (±SD) of quintuplicates (n = 8), and were evaluated using the Statistical Package for Social sciences (SPSS) (IBM SPSS, v 20.0 software, Inc, Chicago IL, USA). Probability at significance level of ($p < 0.05$) was considered as statistically significant.

Table 1
Tensile strength and % elongation of prepared L-Cys-HCl-RTV-Si-TDPs (F1–F6).

L-CyS-HCl: Sorbitol (Formula no.)	Patch thickness (mm)	Tensile strength	
		Maximum stress (S_{max}) MPa	% Elongation at yield point
F1	1.006 ± 0.06	2.96 ± 0.23	350.00 ± 37.55
1:0 (F2)	1.004 ± 0.04[a]	1.49 ± 0.16[c]	270.20 ± 20.39[b]
1:1 (F3)	0.988 ± 0.04[a]	1.40 ± 0.09[c]	273.40 ± 34.25[b]
1:2 (F4)	1.009 ± 0.04[a]	1.39 ± 0.18[c]	292.67 ± 28.39[a]
1:3 (F5)	1.025 ± 0.03[a]	1.27 ± 0.12[c]	334.00 ± 13.89[a]
1:4 (F6)	1.001 ± 0.06[a]	1.22 ± 0.09[c]	356.7 ± 32.54[a]

Statistical Analysis by applying one way ANOVA followed by Post Hoc (Dunnett) comparative test with F1.
[a] Non-significant differences ($p > 0.05$).
[b] Significant differences ($p < 0.05$).
[c] Significant differences ($p < 0.01$).

3. Results and discussion

3.1. Evaluation of the prepared TDPs

3.1.1. Tensile strength and % elongation

Tensile tests enable studying the mechanical properties and providing information about the ability of the patch to withstand rupture. Table 1 illustrates the effect of L-CyS-HCl and sorbitol as plasticizer on physicochemical properties (tensile strength and % elongation) of RTV-Si-TDPs. The results display that, tensile strength and elongation values decreased due to 5% L-CyS-HCl incorporation which was significantly different from (F1) ($p > 0.01$) and ($p > 0.05$), respectively, by applying one way ANOVA followed by Post Hoc (Dunnett) test.

However, a significant decrease in tensile strength values while elevation in elongation values were observed with the increase in sorbitol concentration compared to (F2). The presented results reveal that, incorporation of L-CyS-HCl produced hard and brittle patch. This could be attributed to the integration of drug within polymeric molecules. However, by increasing plasticizer concentration, tensile strength gradually decreased, unlike % elongation that increased with plasticizer. The effect of sorbitol as a plasticizer on the mechanical properties of the formulations has been previously clarified (Gal and Nussinovitch, 2009). Depending on plasticizer type and optimization of its concentration in transdermal drug delivery systems, plasticizers were previously used for preventing film cracking, improving flexibility and processability. Accordingly, plasticizers enhance the resistance and tear strength

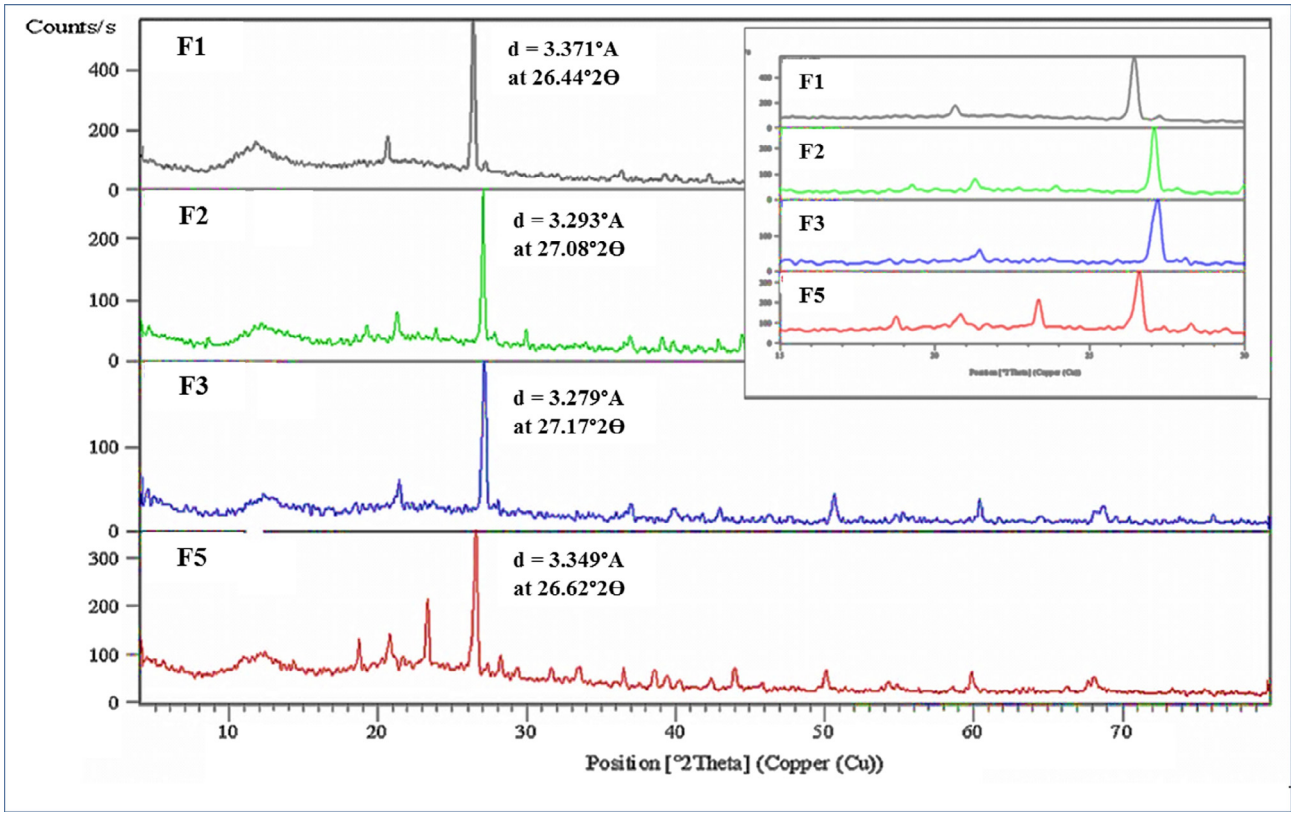

Fig. 2. X-ray diffractograms of different patches revealing the effect of L-CyS-HCl as well as sorbitol concentrations on the x-ray diffraction patterns of silicon patches, illustrating the distance between atomic layers in the polymeric crystal of different patches (d-spacing, d) for plain (—) and 5% L-CyS-HCl loaded RTV-Si-TDPs (—), as well as 5% L-CyS-HCl loaded RTV-Si-TDPs with 1:1 (—) and 1:3 (—) Drug: Sorbitol.

of the polymer film. Upon addition of plasticizer, flexibility of polymer increased as a consequence of loosening of tightness of intermolecular forces by penetration between the polymer chains, disrupting polymer inter-chain cohesive forces and hence, ensuring lubrication of the polymer chains (Höfer and Hinrichs, 2009).

3.1.2. X-ray diffraction

X-ray diffractograms of different patches reveal the effect of L-CyS-HCl as well as sorbitol concentrations on the x-ray diffraction patterns of silicon patches atomic structure, Fig. 2. Using Bragg's law, it can be shown that, the distances between atomic layers in the polymeric crystal of different patches (d-spacing) decreased due to 5% L-CyS-HCl incorporation in the patch matrices from 3.371 Å at 26.44° 2Θ to 3.293 Å at 27.08° 2Θ, for plain and 5% L-CyS-HCl-RTV-Si-TDPs, respectively. The decline in distance between atomic layers in the polymeric crystal (d-spacing) may be due to hydrogen bonding of L-CyS-HCl that could bring atomic layers in the polymeric crystal in more neighboring tighten to each other. The low molecular weight substance can realize strong mutual hydrogen bonding with atomic layers of polymeric crystals in the patches (Gal and Nussinovitch, 2009).

Furthermore, as sorbitol concentration increased the d-spacing increased from 3.279 Å at 27.17 °2Θ to 3.349 Å at 26.62° 2Θ, for F3 and F5, respectively, Fig. 2. Consequently, the effect of sorbitol waged the d-spacing lowering effect of L-CyS-HCl incorporation. The results could be explained by the interposing of the plasticizer between separable strands of polymer, thereby, causing breakdown of polymer–polymer interaction. Subsequently, the tertiary structure of the polymer is distorted into less cohesive structure (Laohakunjit and Noomhorm, 2004), as well, the distances between atomic layers in the polymeric crystal (d-spacing) increase by increasing plasticizer concentration.

3.1.3. Surface properties and porous texture analysis

Fig. 3 illustrates the SEM microphotographs of different RTV-Si-TDPs. The micrographs show that incorporation of L-CyS-HCl as well as sorbitol increased surface porosity of different RTV-Si-TDPs in the following ascending order, F1 < F2 < F3 < F5. The results can be explained on the base of that, the drug and plasticizer interposed between individual strands of the polymer, where the tertiary structure of the polymer was modified into more porous and less cohesive structure (Gal and Nussinovitch, 2009).

3.2. In-vitro release study

Statistical analysis by applying one way ANOVA followed by Post Hoc (Dunnett) comparative test of the mean values of percent L-CyS-HCL released from different L-CyS-HCl-RTV-Si-TDPs after a period of 24 h, (13.75, 14.82, 24.02 and 26.05%) from (F3, F4, F5 and F6), respectively, compared with that released from F2 (11.78%), showed significant differences at ($p > 0.05$), Fig. 4. Moreover, no significant differences were observed by applying *t*-test for comparing the mean values of percent drug released from F3 and F4 as well as F5 and F6. In addition, the calculated *f1* values (difference factor) was (18, 30, 73 and 93) for (F3, F4, F5 and F6), respectively, compared with that of F2 as a reference; indicating that the dissimilarity of the release profiles were escalating with increasing sorbitol concentration.

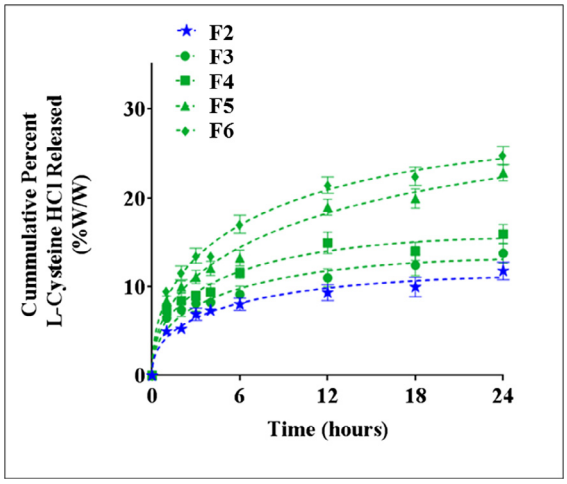

Fig. 4. Effect of Sorbitol concentration on *in-vitro* L-CyS-HCl Released From different RTV-Si-TDPs: in SSPB at (pH 5.5), L-CyS-HCl (F2) (—★—), L-CyS-HCl: Sorbitol 1:1 (F3) (—●—), L-CyS-HCl: Sorbitol 1:2 (F4) (—■—), L-CyS-HCl: Sorbitol 1:3 (F5) (—▲—) and L-CyS-HCl: Sorbitol 1:4 (F6) (—◆—) (Mean ± S.D., n = 3).

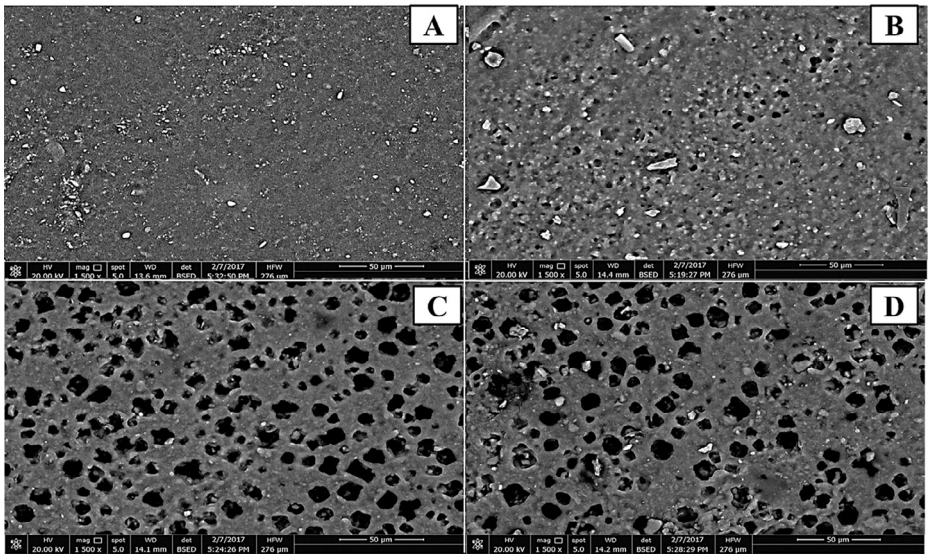

Fig. 3. SEM microphotographs showed the surface porous texture of the RTV-Si-TDPs, (A) plain RTV-Si-TDP (F1), (B) L-CyS-HCl Loaded RTV-Si-TDP (F2), (C) L-CYS HCl: Sorbitol (1:1) Loaded RTV-Si-TDP (F3)and (D) L-CYS HCl: Sorbitol (1:3) Loaded RTV-Si-TDP (F5); X = 1500.

Table 2
In-Vitro L-CyS-HCL release kinetics and mechanisms from L-CyS-HCl loaded RTV-Si-TDPs in SSW3 at (pH 5.4).

L-CyS-HCl: Sorbitol (Formula no.)	Release kinetics						Release mechanisms								R/F (after 24 h)
	Zero order		First oder		Second oder		Diffusion (Higuchi Model)		Korsmeyer–Peppas			Peppas and Sahlin			
	$Q_t = Q_0 - K_0 t$		$\ln Q_t = \ln Q_0 - K_1 t$		$Q_t/Q_\infty\ (Q_\infty - Q_t) = K_2\ t$		$Q_t = K_H\ \sqrt{t}$		$Q_t/Q_o = K_{KP} t^n$			$Q_t/Q_\infty = k_l\ t^m + k_2\ t^{2m}$			
	r^2	K_0 ($C.\ h^{-1}$)	r^2	K_1 (h^{-1})	r^2	K_1 ($C^{-1}.\ h^{-1}$)	r^2	K_H ($h^{-1/2}$)	r^2	n	Kkp (h^{-n})	K1 (% $h^{-0.45}$)	K2 (% $h^{-0.9}$)	r^2	
1:0 (F2)	0.9894	0.2837	0.9919	0.0031	0.9907	0.000034	0.9906	1.6754	0.9836	0.2519	5.2059	5.083	0.1090	0.9861	0.0896
1:1 (F3)	0.9888	0.3022	0.9912	0.0034	0.9902	0.000037	0.9977	1.7829	0.9881	0.2317	6.3768	6.130	0.2042	0.9621	0.1391
1:2 (F4)	0.9889	0.3097	0.9918	0.0035	0.9904	0.000039	0.9967	1.8549	0.9861	0.2136	7.1631	6.858	0.3060	0.9565	0.1865
1:3 (F5)	0.9899	0.6036	0.9948	0.0072	0.9927	0.000085	0.9949	3.9440	0.9858	0.3111	7.7785	7.448	0.8289	0.9843	0.4651
1:4 (F6)	0.9885	0.6436	0.9941	0.0078	0.9916	0.000095	0.9950	4.0551	0.9835	0.3066	9.1264	8.703	1.1394	0.9781	0.5471

k_0 = Zero order release rate constant.
k_1 = First order release rate constant.
k_2 = Second order release rate constant.
k_H = Higuchi release rate constant.
k_{KP} = Korsmeyer–Peppas release rate constant.
t = Release time.
Q_t = Drug released fraction at time t.
Q_o = Initial amount of drug.
n = The parameter that depends on the release mechanism and the shape of the sample tested.
m = Diffusion exponent for Fickian diffusion (0.45).
2m = Diffusion exponent for Anomalous transport (0.9).
r^2 = Correlation Coefficient Squared.
$R/F = (K_2/K_1) \times t^m$.
The underline signify the data that confirm the selected release kinetics and release mechanisms.

Previous studies have indicated that, the release rate of the drug can be accustomed by changing the type and concentration of the plasticizer. This has been explained by the increase in diffusion rate of water-soluble active substance with the increase in plasticizer concentration, which may cause a tortuosity of the drug path due to its high solubility, results in weakening the integrity of the patch matrix. Likewise, increasing the porosity on the patch surface creates more pores that facilitates the drug release (Rahman et al., 2011). Accordingly, plasticizers such as sorbitol can change release rate of the therapeutic components contained in transdermal drug delivery systems.

3.2.1. Release kinetics and mechanism of L-CyS-HCl from L-CyS-HCl-RTV-Si-TDPs

The release profiles of L-CyS-HCl from L-CyS-HCl-RTV-Si-TDPs are demonstrated in Table 2. The release data shows good correlation with first order pattern with r^2 values ≈1, indicating that drug release kinetic was concentration dependent. Fitting the release data to Higuchi model revealed high regression coefficient values ≈1, indicating predominant of diffusion-controlled mechanism of drug release, as presented in Table 2.

The mechanism of L-CyS-HCl release from L-CyS-HCl-RTV-Si-TDPs was studied by applying the Korsmeyer model to the release data up to 60% release. It was revealed that, release of L-CyS-HCl from L-CyS-HCl-RTV-Si-TDPs obeyed a Fickian diffusion model with exponents (n) values <0.45. Further analysis by Peppas and Sahlin model showed higher values of the diffusion constant (k1) compared with the relaxation constant (k2), Table 2. The results indicate the predominance of diffusion mechanism as a mechanism for drug release for all cases in the study. The R/F ratio value for (F2) was very low (0.0896); indicating that drug release mechanism was mainly diffusive, due to highly close tightness of polymeric patch. With increasing plasticizer concentration, F3–F6, the ratio R/F values increased gradually depending on sorbitol concentrations but still less than 1, Table 2. Where increase in plasticizer concentration causes the influence of the diffusion mechanism on drug release less relevant and allowing the matrix to be eroded (Rahman et al., 2011).

3.3. Skin permeation studies

As no significant differences were observed for the percent drug released from (F3 and F4) as well as (F5 and F6); F3 and F5 were selected and compared with F2 for the *ex-vivo* skin permeation study; to clarify the significance of sorbitol effect on the studied parameters and therefore, elucidate and select the optimum formulation.

Effect of the plasticizer content on L-CyS-HCl skin permeation was assessed. Fig. 5 and Table 3 show the permeation profiles as well as permeation parameters of L-CyS-HCl through excised dorsal rat skin from various patches (F2, F3 and F5). The permeation rate (J μg/cm^2/h) of L-CyS-HCl significantly increased ($p < 0.01$) as the sorbitol ratio increased in the patch, with skin permeation rate 2 folds higher in patches containing drug: sorbitol 1:3 (F5) than that in patches containing drug without sorbitol (F2).

The lag time for L-CyS-HCl release is shown in Table 3, where the plasticizer concentration had a significant effect on the observed lag time. This effect on the lag time was probably due to the higher permeability coefficient (Kp) of the drug across the skin by increasing sorbitol concentration, in a reverse order of lag time. The obtained lag time could be explained previously, where after the hydrophilic drugs being released from the polymeric films, they reach skin surface, then pass to the dermal circulation via permeation through cells of epidermis (lipid) and/or through skin appendages (aqueous) (Riviere and Papich, 2001). Thus the delayed drug permeation to the acceptor media could

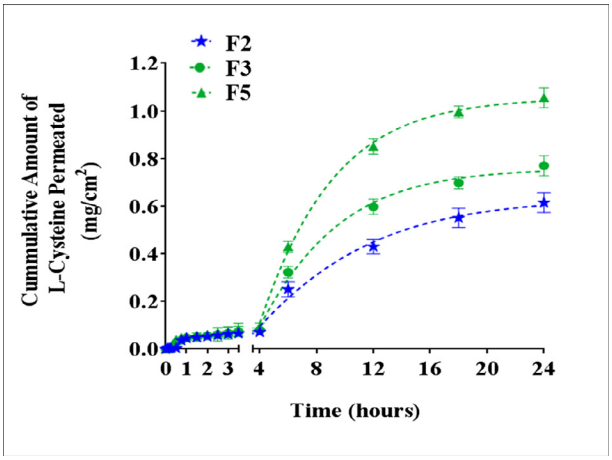

Fig. 5. Permeation profiles of L-CyS-HCl through excised rat skins from various L-CyS-HCl Loaded RTV-Si-TDPs: L-CyS-HCl (F2) (—★—), L-CyS-HCl: Sorbitol 1:1 (F3) (—●—) and L-CyS-HCl: Sorbitol 1:3 (F5) (—▲—) (Mean ± S.D., n = 3).

Table 3
Permeation parameters of L-CyS-HCL through excised dorsal rat skins from various L-CyS-HCL loaded RTV-Si-TDPs.

L-CyS-HCL: Sorbitol	Permeation parameters		
	T_L (h)	J (μg/cm^2/h)	Kp ($\times 10^{-2}$) (cm/h)
1:0 (F2)	3.84 ± 0.28	0.4 ± 0.08	0.08 ± 0.011
1:1 (F3)	3.24 ± 0.34[b]	0.5 ± 0.10[a]	0.1 ± 0.031[c]
1:3 (F5)	3.04 ± 0.20[c]	0.8 ± 0.14[c]	0.16 ± 0.052[c]

T_L: lag time, J: skin permeation rate, Kp: permeability coefficient ± S.D. (n = 3).
[a] Insignificantly different from control (F2) ($p > 0.05$).
[b] Statistically significant different from the control (F2) ($p < 0.05$).
[c] Statistically significant different from the control (F2) ($p < 0.01$).

be a result of the low partition coefficient of the hydrophilic drug; where the penetrating drug must have some propensity to partition into the intercellular lipids of the stratum corneum, (Riviere and Papich, 2001).

As skin permeation rate of water soluble drugs depends on both its solubility and the diffusion in the patch, and as RTV-Si-TDPs are hydrophobic vehicles, thus, it is expected that L-CyS-HCl as a water soluble drug has low affinity to the hydrophobic matrices, which results in high skin permeation rate (J μg/cm^2/h). Having this hydrophobic nature, RTV-Si-TDPs have generally occlusive effect, i.e., they do not allow water to be evaporated from skin surface; a specific effect that increases drug permeation across the skin. Occlusion predominantly increases hydration of stratum corneum, enhances swelling of the corneocytes and increases the intake of water into the intercellular lipid domains. In addition, hydration may facilitate partitioning of the penetrating compound from the stratum corneum to the epidermis. Thus, increases penetration, considering that the permeation is mainly transcellular, because of the hydrophilicity of the drug (Treffel et al., 1992). It has been previously reported that, increase in the plasticizer amount enhances the humidity absorption of the transdermal films, which is closely related to the permeability features of the water soluble drugs through transdermal films (Lade et al., 2011). This may explain the increase in the permeation rate (J μg/cm^2/h) of L-CyS-HCl by increasing sorbitol concentration in the patches.

3.4. In-vivo permeation and pharmacokinetics studies

Formula F5 was selected for in vivo studies depending on the results obtained in ex-vivo skin permeation studies. Where, F5

had the highest skin permeation rate (J), the shortest lag time, as well as, the highest observed permeability coefficient (Kp) of the drug across the skin, compared with the other tested formulations.

Glutathione (GSH) is the most abundant intracellular low molecular weight linear tripeptide of three amino acids: cysteine, glycine and glutamic acid. This tripeptide exists in reduced (GSH) and oxidized (GSSG) forms. The relative amounts of each form determine the cellular redox status (GSH/GSSG ratio) which is often used as a marker of anti-oxidative state of the cells (Jones, 2006). Recently, several studies have shown that a supplementation with N-acetyl cysteine, a cysteine precursor, is an effective strategy to enhance GSH production. Certainly, amino acid (cysteine) is the main factor limiting the synthesis of GSH (Li et al., 2002).

Fig. 6 and Table 4 show the mean plasma concentration-time profiles as well as non-compartmental pharmacokinetic parameters of endogenous-synthesized *in-vivo* GSH in rats, after receiving IV bolus dose of L-CYS-HCl and applying L-CYS loaded RTV-Si-TDPs (F5). After 20 mg IV bolus dose of L-CyS-HCl, GSH plasma concentrations were rapidly increased to 100 μg/ml within 1 h and reached its maximum concentration (C_{max}) 0.42 mg/ml within 5 h (t_{max}), then declined exponentially with an elimination half-life ($t_{1/2}$) of 6.5 h. However, after 80 mg L-CyS-HCl loaded RTV-Si-TDPs application, L-CYS-HCl was slowly absorbed from the site of application followed by *in-vivo* synthesis of endogenous GSH, with elevation in GSH plasma concentration from the base line, within 5 h (lag time).

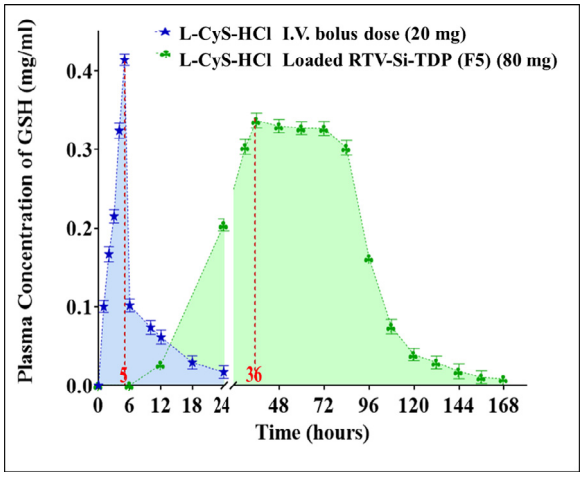

Fig. 6. Mean Plasma concentration-time profiles of GSH in rats after administration of a single I.V. bolus dose (20 mg) of L-CyS-HCl and L-CyS-HCl Loaded RTV-Si-TDP (F5) (≈80 mg L-CyS-HCl). (Mean ± S.D., n = 8).

Table 4
Pharmacokinetic parameters of GSH in rats after IV administration of 20 mg single dose L-CyS-HCL and 80 mg L-CyS-HCL loaded RTV-Si-TDP (F5).

Pharmacokinetic parameters	20 mg (IV)	RTV-Si-TDP (F5)
C_{max} (mg/ml)	0.42 ± 0.035	0.34 ± 0.009
t_{max} (h)	5 ± 0.260	36 ± 3.700
$AUC_{0\rightarrow t}$ (mg·h/ml)	2.25 ± 0.093	26.23 ± 4.250
$AUC_{0\rightarrow\infty}$ (mg·h/ml)	2.4 ± 0.122	26.433 ± 3.800
K (h^{-1})	0.107 ± 0.027	0.037 ± 0.002
$t_{1/2}$ (h)	6.5 ± 0.810	18.9 ± 1.200
MRT (h)	8.9 ± 1.200	64.2 ± 2.700
F	1	2.75 ± 0.130

C_{max} = Maximum drug concentration.
t_{max} = Time to reach C_{max}.
$AUC_{0\rightarrow t}$ = Area under the concentration-time curve from time 0 to t.
$AUC_{0\rightarrow\infty}$ = Area under the concentration-time curve from time 0 to infinity.
K = Elimination rate constant.
$t_{1/2}$ = Elimination Half Life.
MRT = Mean Residence Time.
F = Relative bioavailability of the patch $= \frac{AUCinf(patch)}{AUCinf(I.V.)} \cdot \frac{Dose(I.V.)}{Dose(patch)}$.

As previously determined in L-CyS-HCl skin permeation studies, a lag time of 3.04 h was established for L-CyS-HCl skin permeation from L-CyS-HCl loaded RTV-Si-TDPs, which could be returned to the delayed skin penetration of the hydrophilic L-CyS-HCl, thus slowed the rate for the drug to reach the plasma, followed by a lag time for synthetization of endogenous GSH. Consequently, the rate of endogenous GSH synthesis may be affected. GSH concentrations reached its C_{max} (0.34 mg/ml) with t_{max} around 36 h; subsequently, GSH levels were sustained up to 4 days (application time). GSH concentrations reached a plateau at around 36–96 h. After 96 h of application, the patch was removed which resulted in decline in GSH levels. Unlike IV dosing, elimination half-life ($t_{1/2}$) of GSH after the patch application was longer than that following IV bolus administration. This difference was probably due to the fact that, elimination of GSH following patch application was release rate limiting, meaning that the elimination rate constant (k) was higher than the release/absorption rate (flip-flop). Consequently, comparing the likelihood of the mean residence time (MRT) after both administration routs that was accordingly affected.

The pharmacokinetic profile observed in the study revealed that, L-CyS-HCl loaded RTV-Si-TDPs provided smooth, controlled L-CyS-HCl delivery with a C_{max} of endogenously synthesized GSH, equivalent to the effective doses and a t_{max} that was significantly longer compared with that of L-CyS-HCl IV administration ($p < 0.001$), with no peak fluctuations. Indeed, modeling of steady-state pharmacokinetic data with higher exposure (AUC), Table 4.

Following patch application, the systemic concentrations of GSH remained relatively constant because of rapid L-CyS-HCl deposition into the stratum corneum, which was then steadily delivered into plasma, metabolized in the liver and delivered into plasma as GSH. McPherson and Hardy (2012) have indicated that, as cysteine represents 33.6% of the GSH molecule, 200 mg of cysteine (commercial dosage) would be sufficient for the body to theoretically synthesize up to 600 mg of GSH (McPherson and Hardy, 2012). Consequently, supplementation with of NAC (an antioxidant product) results in 3 folds GSH production endogenously by the body. Therefore, the level of GSH, reduced thiols, increases significantly compared to baseline (0.25 mg/ml endogenous GSH) on NAC administrations. In the meantime, Borgström and Kågedal (1990) have observed the prolongation in t_{max} and a non-linear increase in NAC (C_{max}) and bioavailability (F) after increasing NAC oral doses, which could be explained by the saturation of a capacity-limited systemic elimination process (Borgström and Kågedal, 1990). This finding agrees with the obtained three folds increase in the absolute bioavailability (F) after the patch application compared to that of IV administration.

An outcome that permits greater assurance of GSH cells loading and improves efficacy and access to safely exposure to EMR with simple L-CyS-HCl titration using L-CyS-HCl loaded RTV-Si-TDPs.

3.5. In-vivo evaluation of protective effect of L-CyS-HCl-RTV-Si-TDPs against oxidative stress hazards of mobile phone emitting EMR

Rats received L-CyS-HCL dose ≥30 mg (groups 7, 8 and 9) showed mortality (data not shown). It has been previously clarified that, for therapeutic use, L-CyS-HCL and its prodrugs when administered at high levels are responsible for many side effects, which may be related to the perturbation of extracellular fluid redox status or metabolic acidosis. Wherever, large increases in free thiols in the circulation are associated with thiyl radical-mediated reactions. As well as, destabilizing effects of increasing in thiol/disul-

fide ratios in the plasma, which is normally in a more oxidized state than intracellular compartments. Changes in the thiol redox gradient across cells could also adversely affect any transport or cell signaling processes, depending on the formation and rupture of disulfide linkages in membrane proteins (Deneke, 2001).

Positive control group as well as prophylactic treated groups were similarly exposed to EMR after 2 h post treatment with IV of L-CyS-HCL; while group treated with L-CyS-HCL-RTV-Si-TDPs (F5) was exposed to EMR after 2 days post treatment. Hence, according to the *in-vivo* study, endogenously synthesized GSH concentrations reached its t_{max} at 36 h with a plateau at 36–96 h.

3.5.1. Hematological studies

3.5.1.1. Erythrocyte osmotic fragility test (EOF). Fig. 7 illustrates that, blood samples of different groups (group 1–6) diluted with NaCl concentrations (0% & 0.1%) showed nearly complete hemolysis. At NaCl concentrations, 0.2, 0.3 and 0.4%, positive and negative control groups showed complete hemolysis. While pretreated groups with different L-CyS-HCL concentrations, as an effective antioxidant, revealed protection of erythrocytes from oxidative fragility damage due to ROS produced by EMR in rats in the following order: group 6 ≈ group 5 > 4 > 3, presented as reduction in percent hemolysis with significant difference in percent hemolysis values ($p < 0.05$) compared with negative control groups (group 1), by applying one way ANOVA followed by Post Hock (Dunnett) test for multiple comparison. At NaCl concentration of 0.4%, group 5 and 6 showed 40% protection against hemolysis due to EMR exposure, compared to positive control group (group 2). Starting from 0.5 and ending to 0.9% concentrations of NaCl used for dilution of blood samples of different groups, the percentage hemolysis showed sharp descending with ascending in percent protection against hemolysis (83%, 75%, 80%, 82%, 95% and 94%) for groups (1, 2, 3, 4, 5 and 6) respectively, at NaCl concentration of 0.9%.

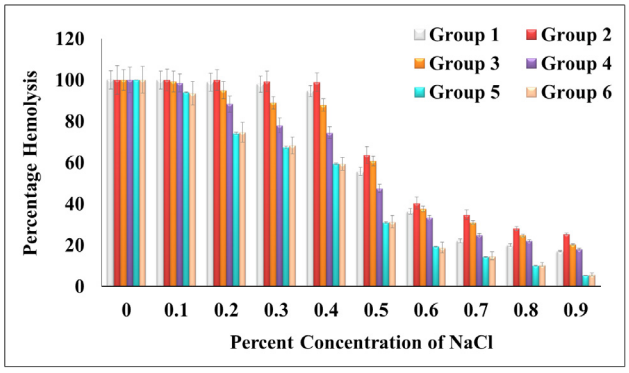

Fig. 7. Effect of L-CyS-HCl concentration on Erythrocyte osmotic fragility (EOF) in rats, indicated as blood hemolysis, after IV administration of a single different concentrations of L-CyS-HCl and exposed to 900 MHz RF/MW continuous fields for four hours (Mean ± S.D., n = 8).

The significant difference in percentage hemolysis, indicative of osmotic fragility, observed between different groups of rats, with lower values in both negative control & prophylactic treated rats compared with positive control group, could be attributed to the enormous ROS produced in the positive control animals as a result of oxidative stress, which is responsible for tissue damage and injurious effects on erythrocyte cytomembrane. It has been found previously that, erythrocyte membrane is rich in polyunsaturated fatty acids which are liable to lipid peroxidation and are responsible of the loss of membrane fluidity, and hence cellular lysis (Brzezińska-Ślebodzińska, 2003). Since oxidative stress occurs when the antioxidant defense systems in the body are stunned by free radicals and enhances the fragility of erythrocyte (Alhassan et al., 2010), L-CyS-HCL administration to experimental rats apparently, reduces the intensity of oxidant stress by enhancing the antioxidant defense mechanisms and minimizing the destruction of erythrocyte.

3.5.1.2. Blood picture. Table 5 shows that, there was a significant effect on rats' blood structure due to the exposure to mobile phone EMR. Values of RBCs, Hb and PLT counts as well as values of HCT, MCV, MCH and MCHC decreased, while LY count increased by exposure to EMR. Positive control (group 2), groups 3 & 4 of rats that received 5 mg, 10 mg of L-CyS-HCL, respectively, and were exposed to EMR showed significant difference in the whole blood picture values compared with their alternatives of negative control (group1). Fruitfully, rats that received 20 mg L-CyS-HCL (I.V.) and L-CyS-HCl-RTV-Si-TDPs (F5), and were exposed to EMR (group 5 & 6), respectively, showed non-significant difference in blood picture values compared to negative control (group 1) ($p < 0.05$) unlike those rats of positive control group.

From a biological point of view, blood can be considered as a tissue comprising various types of cells (RBCs, WBCs, and platelets) and a liquid of intercellular material (plasma) (El-Bediwi et al., 2013). The hypothesis has illustrated that most physiological functions in living organisms are electrochemical in nature; disturbance of intrinsic electrical or chemical process within the cell structure has the potential to disrupt cell function leading to mal-

Table 5
Values of blood picture before and after exposure to mobile phone electromagnetic radiation.

Group	Hb (g/dL) ↓	HCT (Ratio) ↓	RBCS (10^{12}/L) ↓	MCV (FL) ↓	MCH (Pg) ↓	MCHC (g/dL) ↓	LY (%) ↑	PLT (10^9/L) ↓
GP1: Negative control	15.4 ± 0.87	43.5 ± 1.03	9.13 ± 1.03	61.3 ± 1.07	16.9 ± 0.63	29.5 ± 1.73	73.8 ± 2.13	898 ± 62.13
Reference control (Alghamdi and ElGhazaly, 2012)	15.54 ± 0.38	37.26 ± 1.83	9.71 ± 0.34	42.54 ± 0.45	16.28 ± 0.28	30.8 ± 3.89	76.74 ± 3.33	1512.8 ± 271.91
GP2: Positive control	8.7 ± 0.51[d]	29.6 ± 3.57[d]	5.12 ± 0.26[d]	55.8 ± 1.23[b]	8.6 ± 1.07[d]	26.5 ± 2.03[a]	83.5 ± 3.02[c]	620 ± 40.43[d]
GP3: 5 mg (IV)	9.2 ± 0.39[d]	31.6 ± 2.02[d]	5.71 ± 0.39[c]	57.8 ± 2.08[a]	11.23 ± 0.86[c]	26.8 ± 2.17[a]	77.5 ± 2.51[a]	744 ± 42.23[b]
GP4: 10 mg (IV)	10.6 ± 0.42[d]	35.15 ± 1.94[c]	6.07 ± 0.42[c]	60.4 ± 1.93[a]	14.94 ± 1.45[a]	27.9 ± 3.93[a]	75.4 ± 3.2[a]	851 ± 55.5[a]
GP5: 20 mg (IV)	13.2 ± 0.61[b]	42.7 ± 2.56[a]	9.22 ± 1.03[a]	61.1 ± 3.17[a]	16.7 ± 2.37[a]	28.6 ± 2.68[a]	70.8 ± 2.78[a]	890 ± 43.11[a]
GP6: L-CyS-HCl-RTV-Si-TDPs (F5)	14.99 ± 0.85[a]	42.18 ± 1.89[a]	9.13 ± 1.21[a]	61.07 ± 2.11[a]	15.23 ± 2.26[a]	28.33 ± 2.03[a]	68.56 ± 3.13[a]	860 ± 53.35[a]

Hb = Hemoglobin MCH = Mean Corpuscular Hemoglobin.
Hct = Hematocrit MCHC = Mean Corpuscular Hemoglobin Concentration.
RBCs = Red Blood Corpuscles Count % LY = % lymphocytes.
MCV = Mean Cell Volume PLT = Platelets count.
Statistical Analysis by applying one way ANOVA followed by Post Hoc (Dunnett) comparative test with group 1.
[a] Non-significant differences ($p > 0.05$).
[b] Significant differences ($p < 0.05$).
[c] Significant differences ($p < 0.01$).
[d] Significant differences ($p < 0.001$).

function of organ systems. Recently, it has been elucidated that, owing to the effect on electrical charge, EMR may modify ionic structures of elements within cell membrane, distributing the influx and efflux of various elements including calcium ions; with subsequent alteration of cell structure and impairment of cell function, with subsequent tissue disorders and organ dysfunction (Jelodar et al., 2011).

The obtained results were confirmed with those reported previously with significant reductions in the measurements of the blood, as hemoglobin (Hb) and hematocrit (Hct). In addition, the indices of RBCs (RBCs count, MCV, MCH and MCHC) and the average number of platelets (PLT) were noted to be declined by increasing periods of EMR exposure. Hence, the EMR emitted from mobile phones may lead to a clear harmful influence on the cell walls, especially walls of RBCs with an imbalance in blood enzymes (Alghamdi and ElGhazaly, 2012). Moreover, there is a significant influence on hemoglobin molecule structure due to its damage after rats exposure to EMR (El-Bediwi et al., 2013). The decrease in the concentration of hemoglobin could be attributed to the interaction between iron of heme and electromagnetic field, by which magnetic field enters the body and acts on ions in all the vital organs such as spleen, bone marrow, kidney and liver, that alters the cell membrane potential and distribution of ions (Singh et al., 2013).

Blood parameters (HCT, MCV, MCH and MCHC) are most important means by which the decrease in numbers of RBCs could be determined, where the decrease in these parameters' values could be a result of destruction in circulating erythrocytes (Fatayer, 2006). As (HCT) is corresponding to the ratio of RBCs volume to the whole blood volume, this finding could explain the decline in (HCT) values obtained in the study for group 2 compared with group 1, where RBCs volume falls down as a result of EMR exposure with increasing in the plasma volume resulting in decreasing (HCT) values. The obtained diminishing in (MCV) values, the indicator of the RBCs size, was an outcome of RBCs damage due to EMR exposure. As (MCH) is indicative to (Hb) inside RBCs, consequently the decline in both values individually will finally decrease the (MCH) values, as well, (MCHC) is the ratio of (Hb) and (HCT), and hence their diminishing could directly decline (MCHC) values. The obtained results were confirmed with those reported previously; the authors have reported that constant exposure to EMR leads to increasing in Lymphocytes percentage (%LY) associated with lymphatic leukemia, or inflammation of the lymph gland and lymphocytes rising by numerical proliferation, thus cellular mutations occur (Alghamdi and ElGhazaly, 2012).

3.5.1.3. Biological studies.

- ***GSH level determination***

Table 6, illustrates that, glutathione concentration decreased significantly in positive control group (group 2) ($p < 0.001$) compared to negative group (group 1). The results could be attributed to the depletion of glutathione acting as a direct scavenger of ROS. On the other hand, glutathione levels started to replenish in groups of rats treated with L-CyS-HCl (5 & 10 mg) (group 3 and 4). Rats receiving 20 mg of L-CyS-HCl I.V. and L-CyS-HCl-RTV-Si-TDPs (F5) and exposed to EMR (groups 5 and 6), respectively, showed non-significant difference in GSH blood levels compared to the negative control group ($p < 0.05$).

As the endogenous GSH has a protecting role in scavenging radicals and in molecular repair, the depletion of GSH concentration may be owing to the higher consumption of GSH for scavenging the free radicals production due to EMR. However, such scavenging can result in a superoxide-dependent chain production of H_2O_2 and oxidized glutathione, which would stress the cells by oxidation

Table 6
Blood GSH levels and blood serum MDA levels in rats of different groups.

Group number	GSH conc. (mg/ml)	MDA conc. (mMol/L)
Group 1 (negative control)	0.255 ± 0.033	6.12 ± 0.60
Group 2 (positive control)	0.103 ± 0.017[d]	8.75 ± 0.49[d]
Group 3	0.142 ± 0.026[c]	7.52 ± 0.55[b]
Group 4	0.143 ± 0.032[c]	6.88 ± 0.28[a]
Group 5	0.316 ± 0.037[a]	6.48 ± 0.34[a]
Group 6	0.303 ± 0.029[a]	6.28 ± 0.51[a]
Group 1 (negative control)	Unexposed to EMR & untreated with L-CyS-HCl	
Group 2 (positive control)	Exposed to EMR & untreated with L-CyS-HCl	
Group 3	Exposed to EMR & treated with 5 mg of L-CySHCl (IV)	
Group 4	Exposed to EMR & treated with 10 mg of L-CyS-HCl (IV)	
Group 5	Exposed to EMR & treated with 20 mg of L-CyS-HCl (IV)	
Group 6	Exposed to EMR & treated with L-CyS-HCl loaded RTV-Si-TDPs (F5)	
GSH conc.	Glutathione Concentration	
MDA conc.	Malondialdehyde Concentration	

Statistical Analysis by applying one way ANOVA followed by Post Hoc (Dunnett) comparative test with group 1.
[a] Non-significant differences ($p > 0.05$).
[b] Significant differences ($p < 0.05$).
[c] Significant differences ($p < 0.01$).
[d] Significant differences ($p < 0.001$).

(Yurekli et al., 2006). Accumulation of H_2O_2 in the system promotes the Fenton reaction yielding hydroxyl radical ($OH^{\cdot}$). Seriously, $OH^{\cdot}$ is the most reactive and damaging form of ROS that can initiate a chain reaction to generate numerous toxic reactants. Several studies have shown that strategy to enhance GSH production relies on the use of the amino acid cysteine, which is the main factor limiting the synthesis of GSH with effective increasing in GSH levels (Li et al., 2002).

- ***MDA level determination***

In agreement with previous studies (Yurekli et al., 2006), the MDA level increased significantly for positive control rats (group 2) as well as group 3 compared with negative control rats (group 1) ($p < 0.001$) and ($p < 0.05$), as shown in Table 6. On the other hand, groups 4, 5 & 6 treated with L-CyS-HCl conc. of 10 mg & 20 mg and L-CyS-HCl-RTV-Si-TDPs (F5), respectively, showed lower MDA levels in plasma that was non-significantly different from those of negative control (group 1) ($p < 0.05$).

Disturbances of the oxidant/antioxidant balance resulting from the increased production of ROS are contributing factors in the oxidative damage of cellular structures such as lipids, proteins and nucleic acids. In particular, biological membranes that are rich in polyunsaturated fatty acids are the most abundant structures vulnerable to free radicals attack. Therefore, increased blood MDA levels in the study (the potent aldehydic lipid peroxidation products of ω3 and ω6 polyunsaturated fatty acids), might be due to higher rate of oxidative metabolic activity, and higher concentration of readily oxidized membrane polyunsaturated fatty acids, as a result of electromagnetic field emitted from cellular phone. In addition, the peroxidation of lipids is predominantly more harmful leading to a facile propagation of free radicals reactions, where, the fatty acid carbon chain extemporaneously is cleaved during lipid peroxidation process and produces highly toxic pentane, ethane, α, β unsaturated fatty acid aldehydes (Meral et al., 2007).

3.6. Histopathological study

The histopathological examination of different brain tissues of EMR exposed and control rats representing different groups in

Table 7
Histopathological effect of EMR emitted from mobile phones on cerebral cortex, hippocampus and striatum of rat brain after exposure to 900 MHz RF/MW continuous fields for four hours.

Brain location	Group number																	
	Group 1			Group 2			Group 3			Group 4			Group 5			Group 6		
Histopathological alterations	CC.	HP.	S.	CC.	HP.	S.	CC.	HP.	S.	CC.	HP.	S.	CC.	HP.	S.	CC.	HP.	S.
Neuronal degeneration	–	–	–	+++[d]	+++[d]	++[c]	++[c]	+[a]	++[b]	+[a]	+[a]	+[a]	–[a]	+[a]	+[a]	–[a]	+[a]	+[a]
Nuclear pyknosis	–	–	–	+++[d]	+++[d]	++[c]	++[c]	++[c]	++[b]	+ [a]	+[a]	+[a]	–[a]	+[a]	+[a]	–[a]	+[a]	+[a]
Plaques formation			–			+++[d]			++[c]			++[b]			+[a]			+[a]
Group 1 (negative control)													Unexposed to EMR & untreated with L-CyS-HCl					
Group 2 (positive control)													Exposed to EMR & untreated with L-CyS-HCl					
Group 3													Exposed to EMR & treated with 5 mg of L-CyS-HCl (IV)					
Group 4													Exposed to EMR & treated with 10 mg of L-CyS-HCl (IV)					
Group 5													Exposed to EMR & treated with 20 mg of L-CyS-HCl (IV)					
Group 6													Exposed to EMR & treated with L-CyS-HCl loaded RTV-Si-TDPs (F5)					

C.C., Cerebral Cortex; HP, Hippocampus; S., Striatum.
+++ Sever effect (75–100%); ++ Moderate effect (50–75%); + Mild effect (25–50%); – Nil effect (0–25%).
Statistical Analysis by applying Mann-Whitney U independent non-parametric comparative test with group 1.
[a] Non-significant differences ($p > 0.05$).
[b] Significant differences ($p < 0.05$).
[c] Significant differences ($p < 0.01$).
[d] Significant differences ($p < 0.001$).

the study are presented in Table 7. The effect of microwave emitted from mobile phones on *the striatum* of rat brain by exposure to 900 MHz RF/MW fields for continuous four hours is demonstrated in Fig. 8. Group (1) showed no histopathological alterations, Fig. 8-1. The striatum in positive control group (group 2) showed sever focal eosinophilic plaques formation as indicated in Fig. 8-2 and Table 7. Group 3 exhibited intracytoplasmic oedema and vacuolization in some neuronal cells of the striatum, in association with focal eosinophilic plaques formation Fig. 8-3. The striatum in group 4 indicated moderate focal eosinophilic plaques forma-

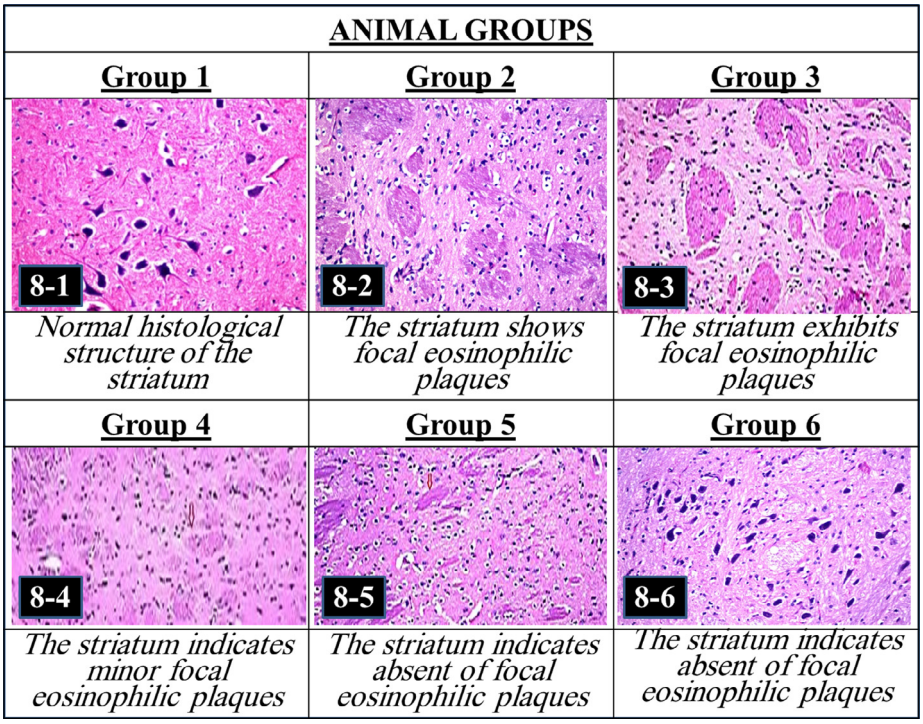

Fig. 8. Photomicrographs showing the effect of microwave emitted from mobile phones on *Striatum* of rat brain after exposure to 900 MHz RF/MW continuous fields for four hours. H & E staining, X = 40.

Group 1 (negative control):	Unexposed to EMR & untreated with L-CyS-HCl
Group 2 (positive control):	Exposed to EMR & untreated with L-CyS-HCl
Group 3:	Exposed to EMR & treated with 5mg of L- CySHCl (IV)
Group 4:	Exposed to EMR & treated with 10mg of L-CyS- HCl (IV)
Group 5:	Exposed to EMR & treated with 20mg of L-CyS-HCl (IV)
Group 6:	Exposed to EMR & treated with L-CyS-HCl loaded RTV-Si-TDPs (F5)

tion, Fig. 8-4. Finally, Figs. 8-5 and 8-6 signify mild focal eosinophilic plaques formation in the striatum of groups 5 & 6.

Statistical study by applying Mann-Whitney U independent non-parametric test revealed high significant difference ($p < 0.001$) for comparing histopathological alterations of positive control group (group 2) with those of negative control group (group 1), Table 7. Significant differences ($p < 0.01$) were detected by comparing obtained data of group 3 pretreated with 5 mg L-CyS-HCL and exposed to EMR with those of negative control group (group 1). However, significant differences ($p < 0.05$) were detected by comparing obtained data of group 4 pretreated with 10 mg L-CyS-HCL and exposed to EMR with those of negative control group (group 1). Fruitfully, non-significant differences ($p > 0.05$) were detected for histopathological alterations of group 5 & 6 pretreated with 20 mg I.V. L-CyS-HCL as well as L-CyS-HCl-RTV-Si-TDPs (F5), respectively, and exposed to EMR compared with those of negative control group (group 1).

Table 7 shows the effect of microwave emitted from mobile phones on the *cerebral cortex* of rat brain by exposure to 900 MHz RF/MW continuous fields for continuous four hours. Group 2 showed marked nuclear pyknosis, degeneration and vacuolization, with cytoplasmic oedema in neurons of the cerebral cortex, which was significantly different from negative control group (group 1) ($p > 0.001$), that exhibited normal histological structure of the meninges and cerebral cortex. Group 3 displayed nuclear pyknosis and degeneration in some neurons, as well, group 4 showed moderate nuclear pyknosis and degeneration in the neurons of the cerebral cortex. Groups 5 & 6 recorded non-significant difference ($p > 0.05$) compared with those of group 1 as cerebral cortex showed normal histological structure, Figure 1-1-Sup up to Figure 1-6-Sup.

The effect of microwave emitted from mobile phones on *the hippocampus (subiculum, fascia dentate & hilus)* of rat brain by exposure to 900 MHz RF/MW fields for continuous four hours is shown in Table 7. Group 1 showed no histopathological alterations with normal hippocampus (subiculum, fascia dentate & hilus). Unlike group 2, nuclear degeneration was detected in the neurons of the both subiculum and fascia dentate in the hippocampus. As well, group 3 showed significant difference ($p > 0.01$) comparing to group 1, as nuclear pyknosis and degeneration were identified in some neurons in subiculum, fascia dentate and hilus of the hippocampus. Group 4, 5 & 6 showed no significant difference ($p > 0.05$) comparing to group 1, as no histopathological alteration was identified in the subiculum, fascia dentate and hilus of the hippocampus, Figure 2-1-Sup up to Figure 2-6-Sup.

The damaged function of EMR on different brain tissues may clarify the histopathological neurotoxicity as edema, vacuolation and plaques observed in the current study. Othman (2012) has suggested that, the lysosomal damage and Nissl bodies destruction as a result of acidophilia are the main causes of edema and chromatolysis in the EMR-exposed rats (Othman, 2012). Recently, the changes in brain tissue that could be caused by thirty minutes exposure to EMF at 940-MHz frequency (mobile phone radiation) have been studied (Razavi et al., 2015). The study revealed increase in apoptotic cells, increase in BBB permeability (albumin leakage from BBB) and increase in BBB space causing changes in the structure of BBB (edema). As the BBB is responsible for the maintenance of the neuronal microenvironment, which is accomplished by separation of the brain from the blood and by selective transport of substances from the blood or brain by the endothelial cells, thus, with changes in BBB structure, neurons life hazarded and finally neuron damaged (Zhao et al., 2007). Ujiie et al. (2003), have verified that, an intact BBB is required for the protection of brain and any deterioration in BBB might disturb the process of blood perfusion and intensifies the probability of plaque formation in the cerebrum (Ujiie et al., 2003).

The obtained histopathological results confirmed the protective effect of L-CyS-HCL against the neuronal damage, resulted from the oxidative effect of ROS induced as a result of EMR emitted from mobile phone exposure. Where, it has been reported that, EMF of cellular phones may affect biological systems, by changing the antioxidant defense systems of tissues, leading to oxidative stress, causing molecular damage to vital structures and functions (Ozguner et al., 2005). It was clarified by Beppu et al. (2015) that, thiol antioxidants may act on the barrier to reinforce the BBB functions by a mechanism involving increasing intracellular GSH and decreasing nuclear factor Kappa B (NF Kappa B) activation (Beppu et al., 2015).

4. Conclusion

On the basis of the findings in the study, an increase in plasticizer concentration (sorbitol) in L-CyS-HCl loaded RTV-Si-TDPs could affect their physical properties and resulted in elongation elevation, while decreased their tensile strength values. In addition, porous patches were resulted and *the in-vitro* L-CyS-HCl release increased owing to sorbitol effect. L-CyS-HCl loaded RTV-Si-TDP (F5) with its optimum physical parameters showed high *ex-vivo* permeation rate through rat's skin. L-CyS-HCl loaded RTV-Si-TDP (F5) showed smooth, controlled *in-vivo* L-CyS-HCl delivery with a C_{max} of endogenously synthetized GSH equivalent to the effective doses and a longer t_{max} compared with that of L-CyS-HCl administration intravenously, with no peak fluctuations. The *in-vivo* study in rats showed mortality for rats received I.V. L-CyS-HCl doses more than 20 mg. Cysteine as the key role precursor of the antioxidant GSH, protected erythrocytes from oxidative damage due to EMR, also prevented erythrocytes fragility in rats, due to ROS produced by 900 MHZ frequency of EMR mimicking mobile phones. Where, L-CyS-HCl loaded RTV-Si-TDP (F5) showed the optimum protection effects. The damaged function of EMR on blood-brain barrier leading to neurotoxicity, highlighted the promising protective effect of L-CyS-HCl loaded RTV-Si-TDP (F5) against neurological disorders and brain dysfunctions. Yet, the results were not enough for scaling up L-CyS-HCl loaded RTV-Si-TDP (F5) for manufacturing. The study strongly recommends further investigations for application on human being against mobile Phone EMR Hazards.

Acknowledgment

The authors gratefully acknowledge Dr. Adel Bakeer, Histology Department, Faculty of Veterinary Medicine, Cairo University, for performing the histopathological examination in this study and his kind assistance in its explanation.

Conflict of interest

None.

This research did not receive any specific grant from funding agencies in the public, commercial, or not-for-profit sectors.

Appendix A. Supplementary material

Supplementary data associated with this article can be found, in the online version, at https://doi.org/10.1016/j.jsps.2018.09.004.

References

Abdel-Rahman, M., 2004. Effect of L-cysteine on blood picture and some serum parameters in rats exposed to 2 Gauss electro-magnetic field. Egypt. J. Hosp. Med. 17, 197–206.

Akerboom, T.P., Sies, H., 1981. Assay of glutathione, glutathione disulfide, and glutathione mixed disulfides in biological samples. In: Methods in Enzymology. Elsevier, pp. 373–382 (Chapter 48).
Alghamdi, M., ElGhazaly, N., 2012. Effects of exposure to electromagnetic field on of some hematological parameters in mice. Open J. Med. Chem. 2 (2), 30–42.
Alhassan, A., Adenkola, A., Yusuf, A., Bauchi, Z., Saleh, M., Ochigbo, V., 2010. Erythrocyte osmotic fragility of Wistar rats administered ascorbic acid during the hot-dry season. J. Cell Animal Biol. 4 (2), 029–033.
Barry, B., 1983. Dermatological Formulations: Percutaneous Absorption. Marcel Dekker, New York, pp. 180–181.
Beppu, M., Sawai, S., Misawa, S., Sogawa, K., Mori, M., Ishige, T., Satoh, M., Nomura, F., Kuwabara, S., 2015. Serum cytokine and chemokine profiles in patients with chronic inflammatory demyelinating polyneuropathy. J. Neuroimmunol. 279, 7–10.
Bernkop-Schnürch, A., Kast, C., Guggi, D., 2003. Permeation enhancing polymers in oral delivery of hydrophilic macromolecules: thiomer/GSH systems. J. Control. Release 93 (2), 95–103.
Bharkatiya, M., Nema, R., Bhatnagar, M., 2010. Designing and characterization of drug free patches for transdermal application. Int. J. Pharm. Sci. Drug Res. 2 (1), 35–39.
Błońska-Sikora, E., Oszczudłowski, J., Witkiewicz, Z., Wideł, D., 2012. Glutathione: methods of sample preparation for chromatography and capillary electrophoresis. Chemik 66 (9), 929–942.
Borgström, L., Kågedal, B., 1990. Dose dependent pharmacokinetics of N-acetylcysteine after oral dosing to man. Biopharm. Drug Dispos. 11 (2), 131–136.
Brzezińska-Ślebodzińska, E., 2003. Species differences in the susceptibility of erythrocytes exposed to free radicals in vitro. Vet. Res. Commun. 27 (3), 211–217.
Deneke, S.M., 2001. Thiol-based antioxidants. Curr. Top. Cell. Regul. 36, 151–180.
El-Bediwi, A.B., Saad, M., El-kott, A.F., Eid, E., 2013. Influence of electromagnetic radiation produced by mobile phone on some biophysical blood properties in rats. Cell Biochem. Biophys. 65 (3), 297–300.
Entzian, P., 1998. Antioxidative and clinical effects of high-dose N-acetylcysteine in fibrosing alveolitis. Adjunctive therapy to maintenance immunosuppression. Pneumologie 52 (7), 396–397.
Fatayer, A., 2006. Hematology (theoretical and practical) culture library house for publication and distribution. J. Environ. Stud. 2, 223–229.
Gal, A., Nussinovitch, A., 2009. Plasticizers in the manufacture of novel skin-bioadhesive patches. Int. J. Pharm. 370 (1), 103–109.
Guney, M., Ozguner, F., Oral, B., Karahan, N., Mungan, T., 2007. 900 MHz radiofrequency-induced histopathologic changes and oxidative stress in rat endometrium: protection by vitamins E and C. Toxicol. Ind. Health 23 (7), 411–420.
Höfer, R., Hinrichs, K., 2009. Additives for the manufacture and processing of polymers. In: Eyerer, P., Weller, M. (Eds.), Polymers-Opportunities and Risks II. Springer, pp. 97–145.
Jackson, P., Blythe, D., 2013. Theory Practice of Histological Techniques. Churchill Livingstone of Elsevier, Philadelphia, pp. 386–431 (Chapter 18).
Jelodar, G., Nazifi, S., Nuhravesh, M., 2011. Effect of electromagnetic field generated by BTS on hematological parameters and cellular composition of bone marrow in rat. Comp. Clin. Pathol. 20 (6), 551–555.
Jones, D.P., 2006. Redefining oxidative stress. Antioxid. Redox Signal. 8 (9–10), 1865–1879.
Kerman, M., Senol, N., 2012. Oxidative stress in hippocampus induced by 900 MHz electromagnetic field emitting mobile phone: protection by melatonin. Biomed. Res. 23 (1), 147–151.
Klemm, M., Troester, G., 2006. EM energy absorption in the human body tissues due to UWB antennas. Progr. Electromagn. Res. 62, 261–280.
Korsmeyer, R.W., Gurny, R., Doelker, E., Buri, P., Peppas, N.A., 1983. Mechanisms of solute release from porous hydrophilic polymers. Int. J. Pharm. 15 (1), 25–35.
Lade, U.B., Amgaonkar, Y.M., Chikhale, R.V., Biyani, D.M., Umekar, M.J., 2011. Design, formulation and evaluation of transdermal drug delivery system of budesonide. Pharmacol. Pharm. 2 (3), 199–211.
Laohakunjit, N., Noomhorm, A., 2004. Effect of plasticizers on mechanical and barrier properties of rice starch film. Starch-Stärke 56 (8), 348–356.
Li, J., Wang, H., Stoner, G.D., Bray, T.M., 2002. Dietary supplementation with cysteine prodrugs selectively restores tissue glutathione levels and redox status in protein-malnourished mice. J. Nutr. Biochem. 13 (10), 625–633.
Marques, M.R., Loebenberg, R., Almukainzi, M., 2011. Simulated biological fluids with possible application in dissolution testing. Dissolution Technol. 18 (3), 15–28.
McPherson, R.A., Hardy, G., 2012. Cysteine: the Fun-Ke nutraceutical. Nutrition 28 (3), 336–337.
Meral, I., Mert, H., Mert, N., Deger, Y., Yoruk, I., Yetkin, A., Keskin, S., 2007. Effects of 900-MHz electromagnetic field emitted from cellular phone on brain oxidative stress and some vitamin levels of guinea pigs. Brain Res. 1169, 120–124.
Moore, J.W., 1996. Mathematical comparison of dissolution profiles. Pharm. Technol. 20, 64–75.
Othman, A., 2012. Effect of electromagnetic radiation exposure on histology and DNA content of the brain cortex and hypothalamus of young and adult male albino rats. J. Radiat. Res. Appl. Sci. 5 (1), 1–20.
Ozguner, F., Altinbas, A., Ozaydin, M., Dogan, A., Vural, H., Kisioglu, A.N., Cesur, G., Yildirim, N.G., 2005. Mobile phone-induced myocardial oxidative stress: protection by a novel antioxidant agent caffeic acid phenethyl ester. Toxicol. Ind. Health 21 (7–8), 223–230.
Ozgur, E., Güler, G., Seyhan, N., 2010. Mobile phone radiation-induced free radical damage in the liver is inhibited by the antioxidants N-acetyl cysteine and epigallocatechin-gallate. Int. J. Radiat Biol. 86 (11), 935–945.
Patel, D., Chaudhary, S.A., Parmar, B., Bhura, N., 2012. Transdermal drug delivery system: a review. Pharma Innovation 1 (4), 66–75.
Peppas, N.A., Sahlin, J.J., 1989. A simple equation for the description of solute release. III. Coupling of diffusion and relaxation. Int. J. Pharm. 57 (2), 169–172.
Raghavendra, K., Doddayya, H., Patil, S., Habbu, P., 2000. Comparative evaluation of polymeric films for transdermal application. Eastern Pharmacist 43, 109–112.
Rahman, M., Ahsan, Q., Jha, M.K., Ahmed, I., Rahman, H., 2011. Effect of mannitol on release of lamivudine sustained release matrix tablets using methocel K15M CR polymer. Inventi. Impact Pharm. Tech. 1, 58–62.
Razavi, M.K., Raji, A.R., Maleki, M., Dehghani, H., Haghpeima, A., 2015. Histopathological and immunohistochemical study of rat brain tissue after exposure to mobile phone radiation. Comp. Clin. Pathol. 24 (5), 1271–1276.
Riviere, J.E., Papich, M.G., 2001. Potential and problems of developing transdermal patches for veterinary applications. Adv. Drug Deliv. Rev. 50 (3), 175–203.
Rover, J.L., Kubota, L.T., Höehr, N.F., 2001. Development of an amperometric biosensor based on glutathione peroxidase immobilized in a carbodiimide matrix for the analysis of reduced glutathione from serum. Clin. Chim. Acta 308 (1–2), 55–67.
Shaikh, S., Birdi, A., Qutubuddin, S., Lakatosh, E., Baskaran, H., 2007. Controlled release in transdermal pressure sensitive adhesives using organosilicate nanocomposites. Ann. Biomed. Eng. 35 (12), 2130–2137.
Singh, H., Kumar, C., Bagai, U., 2013. Effect of electromagnetic field on red blood cells of adult male swiss albino mice. Int. J. Theor. Appl. Sci. 5 (1), 175–182.
Treffel, P., Muret, P., Muret-D'Aniello, P., Coumes-Marquet, S., Agache, P., 1992. Effect of occlusion on in vitro percutaneous absorption of two compounds with different physicochemical properties. Skin Pharmacol. Physiol. 5 (2), 108–113.
Tsai, C.-Y., Chang, C.-C., 2013. Auto-adhesive transdermal drug delivery patches using beetle inspired micropillar structures. J. Mater. Chem. B 1 (43), 5963–5970.
Ujiie, M., Dickstein, D.L., Carlow, D.A., Jefferies, W.A., 2003. Blood–brain barrier permeability precedes senile plaque formation in an Alzheimer disease model. Microcirculation 10 (6), 463–470.
Wang, W.-Y., Hui, P.C., Wat, E., Ng, F.S., Kan, C.-W., Lau, C., Leung, P.-C., 2016. Enhanced transdermal permeability via constructing the porous structure of poloxamer-based hydrogel. Polymers 8 (11), 406–417.
Yildiz, D., Arik, M., Cakir, Y., Civi, Z., 2009. Comparison of N-acetyl-L-cysteine and L-cysteine in respect to their transmembrane fluxes. Biochem. (Moscow) Suppl. Ser. A: Membr. Cell Biol. 3 (2), 157–162.
Yurekli, A.I., Ozkan, M., Kalkan, T., Saybasili, H., Tuncel, H., Atukeren, P., Gumustas, K., Seker, S., 2006. GSM base station electromagnetic radiation and oxidative stress in rats. Electromagn. Biol. Med. 25 (3), 177–188.
Zhao, T.-Y., Zou, S.-P., Knapp, P.E., 2007. Exposure to cell phone radiation up-regulates apoptosis genes in primary cultures of neurons and astrocytes. Neurosci. Lett. 412 (1), 34–38.
Zhu, Y., Gao, F., Yang, X., Shen, H., Liu, W., Chen, H., Jiang, X., 2008. The effect of microwave emmision from mobile phones on neuron survival in rat central nervous system. Progr. Electromagn. Res. 82, 287–298.